Ab initio study of MgH2: Destabilizing effects of selective substitutions by transition metals

Adel F. Al Alam, Samir F. Matar, Naïm Ouaïni

Solid State Sciences; accepted July 22nd 2014

Ab initio study of MgH_2: destabilizing effects of selective substitutions by transition metals.

Adel F. Al Alam [a,b*], Samir F. Matar[c,d], Naïm Ouaini[a].

[a] Holy Spirit University of Kaslik, USEK, P.O. Box 446, Jounieh, Lebanon

[b] University of Balamand, Department of Physics, P.O. Box 100, Tripoli, Lebanon

[c] CNRS, ICMCB, UPR 9048, F-33600 Pessac, France

[d] Université de Bordeaux, ICMCB, UPR 9048, F-33600 Pessac, France

Corresponding author: adelalalam@usek.edu.lb

Abstract:

The strong iconicity of H within rutile MgH_2 is reduced by selective substitution of Mg by *T* (= Fe, Co, Ni, Pd, Pt) using trirutile super-structure host TMg_2H_6. These novel model systems, as computed in the quantum mechanical framework of density functional theory, showed a gradual decrease of the charges carried by H down to –0.02*e* improving the use of MgH_2 for applications.

Keywords:

A. intermetallics. B. bonding. C. interstitial content. E. electronic structure calculation.

1. Introduction

Hydrogen storage materials such as hydrides are leading candidates for clean energy in the future. Archetype hydride MgH_2 has been studied intensively owing to its large gravimetric density ~7.6 wt.%. However, its high thermodynamic stability prevents hydrogen absorption/desorption at mild conditions, whence the difficulty of its *ad hoc* use in applications. Experimental and theoretical efforts have culminated over decades to overcome the latter intricacy. The kinetics of hydrogenation were improved experimentally either by the addition of catalysts [1, 2, 3] or by the introduction of nickel as an adjoined metal such as in Mg_2NiH_4 [4]. Recent theoretical investigations suggested the insertion of light elements such as carbon and boron which decreased the largely ionic character of hydrogen in $(B,C)_{0.167}MgH_2$ [5].

The aim of the present study is to remedy the situation prohibiting the use of MgH_2 in devices by selective substitution of Mg with transition metals (T = Fe, Co, Ni, Pd, Pt) in a trirutile host super-structure using first-principles density functional theory (DFT) calculations [6, 7].

2. Structural details

As illustrated in Fig. 1, ordered trirutile $T Mg_2H_6$ crystallizes as rutile with the tetragonal structure in space group $P4_2/mnm$ (No. 136). Given in Wyckoff letter, T atoms occupy 2a sites at coordinates (0, 0, 0), and Mg atoms are found in 4e sites at (0, 0, z~1/3). There are two hydrogen sub-lattices, namely H1 at 4f (x, x, 0) and H2 at 8j (x, x, z). Both Mg and T species are surrounded by irregular H octahedra. Successive T-H planes (at z = 0 and z = 1/2) are separated by two Mg-H planes (at z~1/6 and z~1/3).

Archetype MgH_2 crystallizes with the tetragonal rutile structure in space group $P4_2/mnm$ (No. 136). The latter order can be compared to the trirutile structure by substituting T species by Mg at 2a sites, whereby H atoms are located exclusively at 4f sites.

3. Computational methodology

Geometry optimization and total energy calculations were performed with the Vienna ab initio simulation package (VASP) [8, 9]. The ion-electron interactions were described using the projector augmented wave (PAW) method [9, 10]. Electron exchange-correlation functionals were built within the generalized gradient approximation (GGA)

scheme following the nonlocal correction of Perdew, Burke and Ernzerhof (PBE) [11]. It is important to mention that semi-core *p* states where accounted for PAW potentials of Mg in order to obtain the correct physical bulk properties and electronic structures for *T*Mg_2H_6 models. The conjugate-gradient algorithm [12] is used in this computational scheme to relax the atoms and to optimize the structural parameters until the forces on all the unconstrained atoms were less than 0.02 eV/Å and all stress components were less than 0.003 eV/Å^3. The tetrahedron method with Blöchl corrections [10] and a Methfessel-Paxton [13] Gaussian smearing scheme were applied for both geometry relaxation and to accelerate the total energy calculations. Brillouin-zone (BZ) integrals were approximated using the special *k*-point sampling. The calculations are converged at an energy cut-off of 404 eV for the plane-wave basis set with respect to the *k*-point integration with a starting mesh of 4×4×4 up to 8×8×8 for best convergence and relaxation to zero strains.

In this work, the atomic charge of hydrogen is calculated using a Bader charge analysis [14]. The latter approach partitions the continuous electron density into region bounded by the minima of the charge density. Such an analysis can be useful when trends between similar compounds are examined; it does not constitute a tool for evaluating absolute ionizations. Bader's analysis is done using a fast algorithm operating on a charge density grid [15]. The results of computed charges *Q* are such that they lead to neutrality when the respective multiplicities are accounted for.

4. Results and discussions

4.1 Geometry optimization, cohesive energies and hydrogen charge density

In as far as *T*Mg_2H_6 models are novel theoretical models chosen herein, geometry optimization was firstly performed. Starting and optimized structural parameters are given in Table 1. Rutile-type MgH_2 was also examined to establish trends of stability for the computed *T*Mg_2H_6 models. The calculated structural parameters for MgH_2 are within 2% of the experiment. All *T*Mg_2H_6 models relaxed in the trirutile structure. The stability of these models can be examined from the computed total electronic energies given in Table 2.

The cohesive energies of various *T*Mg_2H_6 structures were calculated with the expression

$$E_{\text{coh.}} = E(T_2\text{Mg}_4\text{H}_{12}) - 2E(T) - 4E(\text{Mg}) - 6E(\text{H}_2)$$

The energy terms on the right-hand side of the equation represent, in order, trirutile hydride model, pure *T* metal, pure Mg, and gas-phase hydrogen. The strength of cohesive energy of a model is a measure of the stability of that model. Largely negative $E_{coh.}$ indicate stable binding, whereas positive energies correspond to an unstable model. The energy of the gas-phase hydrogen dimer was calculated with an 8×8×8 cell. The cohesive energy per H_2 of MgH_2 is calculated within 8% of the experimental value –0.79 eV [17]. The computed $E_{coh.}$ per H_2 values in Table 2 clearly indicate that all TMg_2H_6 models are stable owing to the negative values. Compared to MgH_2, all models are less stable. The latter finding meets with the aims of this study in as far as less thermodynamically stable hydrides are sought.

The latter should be comforted further by examining the atomic charge of hydrogen shown as a function of *T* species in Fig. 2. As expected, hydrogen exhibits a less ionic character near *T* elements (H1 sub-lattice) compared to H charges near Mg (H2 sub-lattice). This can be explained by the electronegativity value of the different species given in the Pauling scale: χ(Mg) = 1.31, χ(Fe) = 1.83, χ(Co) = 1.88, χ(Ni) = 1.91, χ(Pd) = 2.2, and χ(Pt) = 2.28. All *T* elements are more electronegative than Mg, whence the less ionic hydrogen in their surroundings. Furthermore, H1 charge near *T* elements undergoes gradual reduction of its ionic character from $H^{-\,0.4}$ for $FeMg_2H_6$ model down to $H^{-\,0.02}$ for $PtMg_2H_6$. The latter value is also due to the large H1-Pt separation $d_{H1\text{-}Pt}$ = 1.80 Å. The other hydrogen sub-lattice, namely H2, exhibits a constant evolution around a charge of -6*e*. Nevertheless the overall changes brought by *T* are established. This substantial reduction of the carried charge by H predicted theoretically should be an indication of the readiness of H desorption experimentally. It is important to mention that smaller amounts of metal would be needed to strongly modify MgH_2 especially with platinum which is an expensive metal. Tests are underway with experimental groups at our Institute.

Further we comment on the relative changes of charges on *T* using the Bader charge analysis. The values are as follows:

Fe+0.71; Co: +0.50: Ni: +0.52: Pd: 0.27; Pt: +0.13. The ionization degree follows closely the electronegativity magnitude with the following trend: the least electronegative is the least charged.

4.2 Electronic density of states: DOS analysis

Fig. 3 shows the site projected density of states (PDOS) corresponding to Mg_3H_6 and TMg_2H_6. The energy along the abscissa axis is brought to E_V, top of the valence band (VB) which is separated from the conduction band (CB) by a band gap of ~3.5 eV for trirutile-Mg_3H_6 (Figs. 3a and b). This agrees with the insulating character of archetype MgH_2 showing a band gap of ~5.6 eV [18]. The VB is dominated by H (H1 and H2) with prevailing H2 intensities due to their higher multiplicity with respect to H1. Magnesium PDOS are dominating within the CB due to their low filling and electron departure towards H.

The DOS's of TMg_2H_6 show a few similar feature with MgH_2-like DOS within the 8 eV range from –2 to –10 eV (Figs. 3c,d,e). Similar DOS skylines are also observed within the CB between itinerant *T* states and the Mg/H states. The band gap has decreased down to ~2.5 eV for Fe due to the covalent character brought in by iron. From Co to Ni and Pt the extra electrons brought by the increasing Z number shifts E_F to the states Mg and H formerly found within the CB. However the doping is far too high and leads to closing of the gap. A peculiar feature appears for the localized (sharp) *T* n*d*-states PDOS which signals little mixing with the host Mg and H states and could be labeled as non bonding, as shown by the small PDOS magnitude of Mg and H below the Fe(*d*) PDOS for instance. The insulating character is preserved is as far as the energy is still referred the top of the VB but the gap is much reduced down to ~0.3 eV. Clearly the amount of transition metal is too large ($FeMg_2H_6 \equiv Fe_{0.333}Mg_{0.6667}H_2$) by experimental standards. Note that some of the other transition elements candidates have shown total metallization, *i.e.* a closing of the band gap. Then smaller amounts of *T* elements should be introduced in order to preserve the insulating properties of MgH_2 and future works are planned. Nevertheless, our approach using trirutile host structure has shown relevant effects brought by *T* substitution on the electronic structure of MgH_2 owing to the use of trirutile super-structure allowing selective substitutions of Mg.

5. Conclusion

The use of trirutile host super-structure allowed selective substitution of Mg by *T* elements. This brought significant effects relevant to the reduction of the strong ionic character of H which prohibited the use of rutile MgH_2 in applications. The introduction of *T* species tends to narrow down the band gap of MgH_2 leading to total metallization. Then smaller amounts

should be introduced in order to preserve the insulating properties of MgH_2 as future works are planned.

6. Acknowledgement

We acknowledge financial support from French-Lebanese CEDRE project and CSR-USEK. Part of the calculations where done on MCIA super computers of the University Bordeaux 1. Support from the Conseil Régional d'Aquitaine is gratefully acknowledged.

7. References

[1] D.W. Zhou, J.S. Liu, S.H. Xu, G.Y. Chen, Mater. Sci-Poland 28 (2010) 229.

[2] C.Z. Wu, P. Wang, X. Yao, C. Liu, D.M. Chen, G.Q. Lu, H.M.Cheng, J. Alloys Comp. 420 (2006) 278.

[3] M. Nakhl, M. Zakhour, Ch. Amine, H. El-Rassy, S.F. Matar, Adv. Mater. Res. 324 (2011) 119.

[4] J. Huot, J.F. Pelletier, G.Liang, M. Sutton, R. Schulz, J. Alloys Comp. 330-322 (2002) 727.

[5] S.F. Matar, Comp. Mater. Sci. 69 (2013) 424.

[6] P. Hohenberg, W. Kohn, Phys. Rev. B 136 (1964) 864.

[7] W. Kohn, L.J. Sham, Phys. Rev. A 140 (1965) 1133.

[8] G. Kresse, J. Furthmüller, Phys. Rev. B 54 (1996) 11169.

[9] G. Kresse, J. Joubert, Phys. Rev. B 59 (1999) 1758.

[10] P. E. Blöchl, Phys. Rev. B 50 (1994) 17953.

[11] J. Perdew, K. Burke, M. Ernzerhof, Phys. Rev. Lett. 77 (1996) 3865.

[12] W.H. Press, B.P. Flannery, S.A. Teukolsky, W.T. Vetterling, Numerical Recipes, Cambridge University Press, New York (1986).

[13] M. Methfessel, A. T. Paxton, Phys. Rev. B 40 (1989) 3616.

[14] R. Bader Chem Rev 91 (1991) 893

[15] W. Tang, E. Sanville, G. Henkelman, J. Phys.: Condens. Matter, 21 (2009) 084204. http://theory.cm.utexas.edu/henkelman/research/bader

[16] P. Villars, L.D. Calvert, Peason's Handbook of Crystallographic Data for Intermetallic Phases, 2nd ed., American Society for Metals, Materials Park, OH, 1986.

[17] M. Yamaguchi, E. Akiba, Materials Science and technology,vol. 3B, VHC, New York, 1994, p. 333.

[18] C. Moysés Araújo, S. Lebègue, O. Eriksson, B. Arnaud, M. Alouani, R. Ahuja, J. Appl. Phys. 98 (2005) 096106.

Table 1: Optimized and (starting experimental when available) structural parameters for MgH_2 and TMg_2H_6 models. The distance separating H1 sublattice from *T* element is also given.

Structure	**Unit Cell (Å)**			**Positional parameters**		
	A	***c/a***		***x***	***Y***	***Z***
MgH_2 (rutile)	4.42 (4.516)	0.676 (0.669)	Mg(2*a*)	0 (0)	0 (0)	0 (0)
			H (4*f*)	0.304 (0.306)	0.304 (0.306)	0 (0)
Mg_3H_6 (trirutile)	4.43	1.436	Mg(4*e*)	0	0	0.333
			Mg(2*a*)	0	0	0
			H1 (4*f*)	0.304	0.304	0
			H2 (8*j*)	0.304	0.304	0.333
$FeMg_2H_6$	4.252	1.924	Mg(4*e*)	0	0	0.329
			Fe (2*a*)	0	0	0
			H1 (4*f*)	0.267	0.267	0
$d_{H1\text{-}Fe}$=1.64 Å			H2 (8*j*)	0.313	0.313	0.362
$CoMg_2H_6$	4.263	1.912	Mg(4*e*)	0	0	0.328
			Co (2*a*)	0	0	0
			H1 (4*f*)	0.266	0.266	0
$d_{H1\text{-}Co}$=1.64-1.66 Å			H2 (8*j*)	0.313	0.313	0.364
$NiMg_2H_6$	4.262	2.002	Mg(4*e*)	0	0	0.328
			Ni (2*a*)	0	0	0
			H1 (4*f*)	0.267	0.267	0
$d_{H1\text{-}Ni}$=1.54-1.61 Å			H2 (8*j*)	0.312	0.312	0.360
$PdMg_2H_6$	4.351	2.032	Mg(4*e*)	0	0	0.328
			Pd (2*a*)	0	0	0
			H1 (4*f*)	0.280	0.280	0
$d_{H1\text{-}Pd}$=1.66-1.73 Å			H2 (8*j*)	0.306	0.306	0.351
$PtMg_2H_6$	4.364	2.059	Mg(4*e*)	0	0	0.327
			Pt (2*a*)	0	0	0
			H1 (4*f*)	0.277	0.273	0
$d_{H1\text{-}Pt}$=1.66-1.80 Å			H2 (8*j*)	0.307	0.307	0.356

Table 2: Total electronic energies and cohesive energies in units of eV for all $T\mathrm{Mg_2H_6}$ models.

Structure	$E(T_2\mathrm{Mg_4H_{12}})$	$E(T)$	$E(\mathrm{Mg})$	$E(\mathrm{H_2})$	$E_{\mathrm{coh.}}$	$E_{\mathrm{coh.}}/_{\mathrm{H2}}$
$\mathrm{MgH_2}$ (rutile)	–17.570		–1.487	–6.52	–1.556	–0.778
$\mathrm{FeMg_2H_6}$	–64.517	–7.813	–1.487	–6.52	–3.823	–0.637
$\mathrm{CoMg_2H_6}$	–61.742	–6.810	–1.487	–6.52	–3.054	–0.509
$\mathrm{NiMg_2H_6}$	–57.907	–5.725	–1.487	–6.52	–1.389	–0.232
$\mathrm{PdMg_2H_6}$	–56.832	–5.360	–1.487	–6.52	–1.044	–0.174
$\mathrm{PtMg_2H_6}$	–59.140	–5.366	–1.487	–6.52	–3.340	–0.557

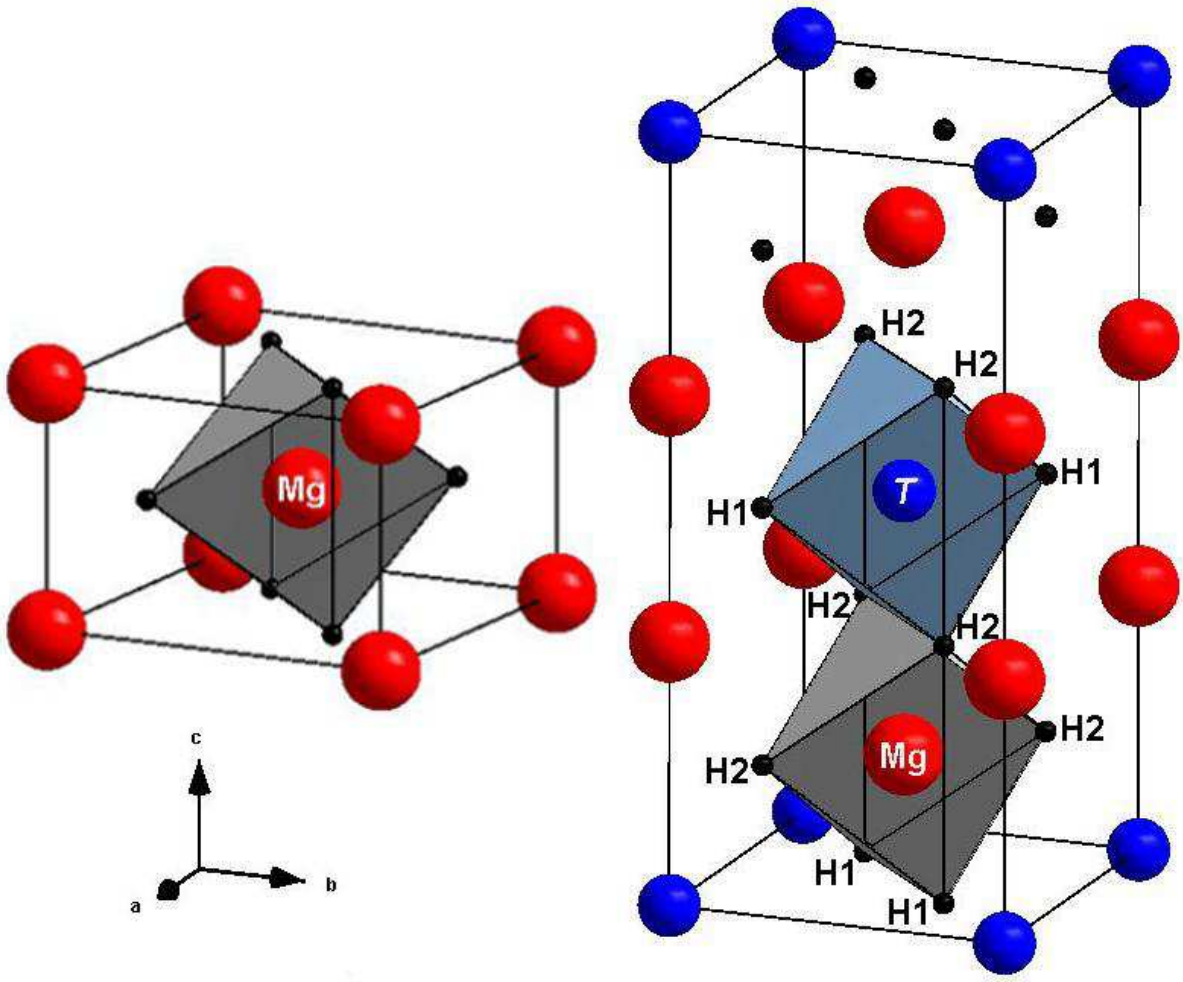

Fig. 1: (Color online) Sketches of the crystal structures of rutile-type $\mathrm{MgH_2}$ (left-hand side) and trirutile-type $T\mathrm{Mg_2H_6}$ (right-hand side).

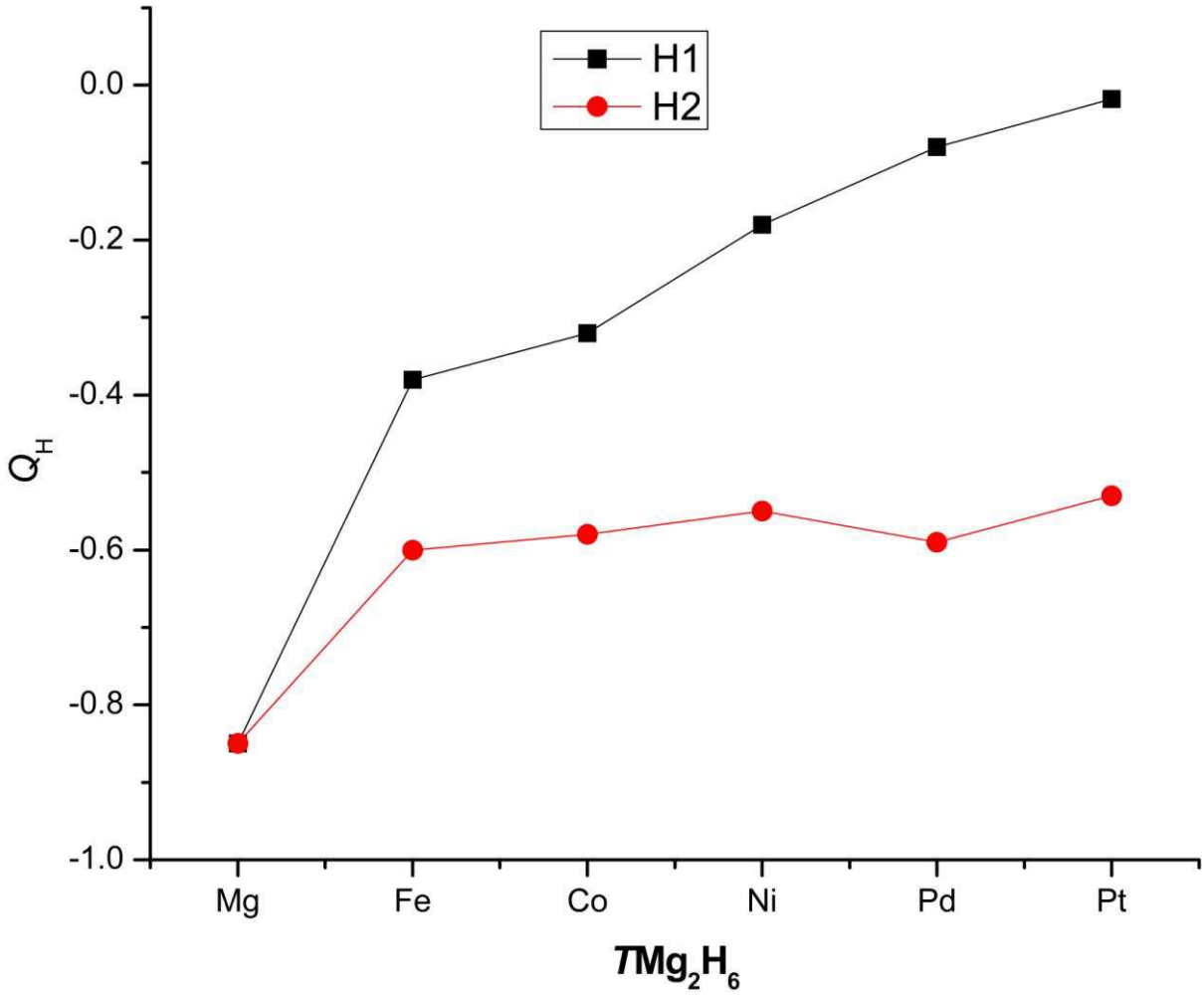

Fig. 2: (Color online) Atomic charge of hydrogen Q_H as function of T species in all $T\mathrm{Mg_2H_6}$ models for H1 and H2 sub-lattices. All values of Q_H are given as a multiple of elementary charge (e = 1.6 × 10^{-19} C).

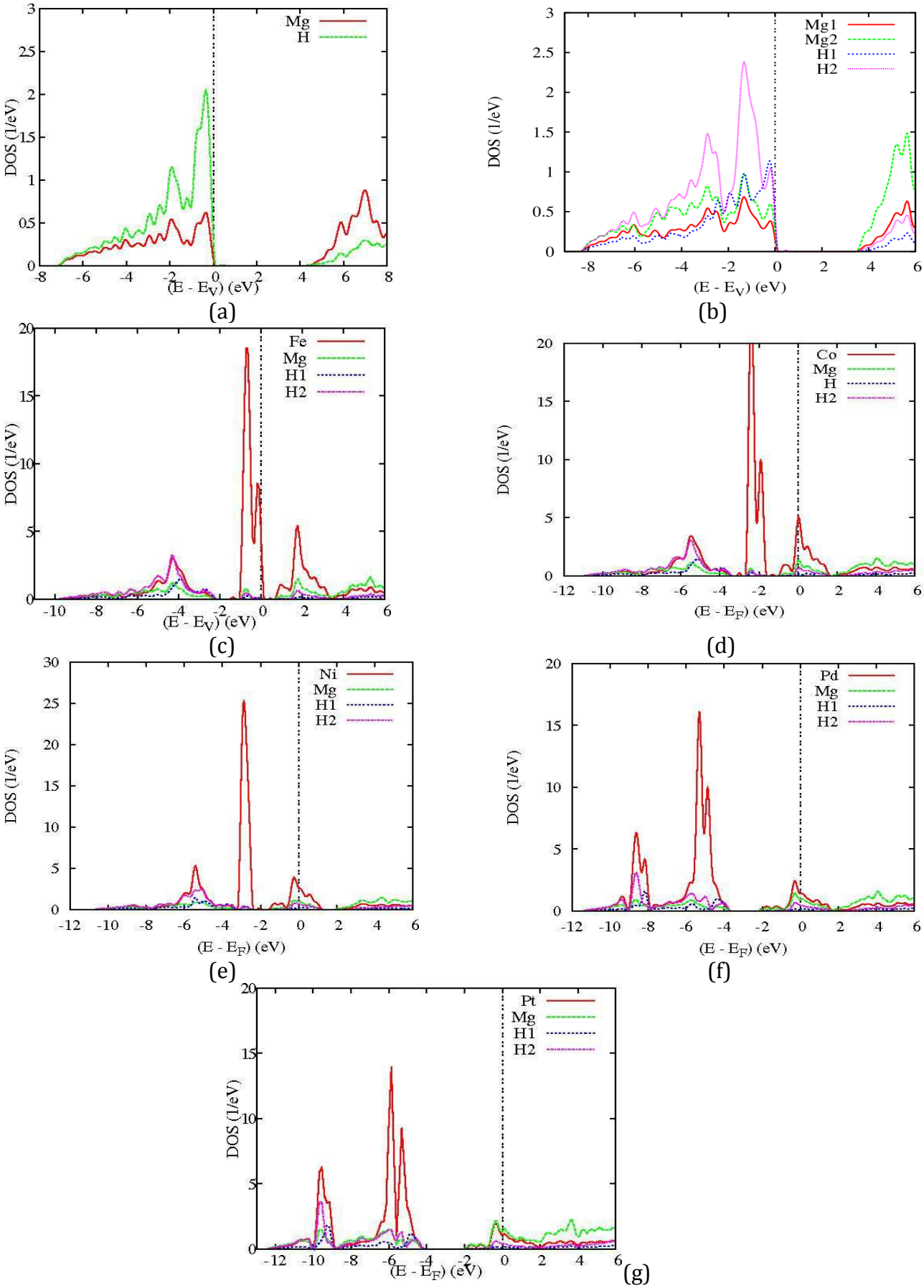

Fig. 3: (Color online) Site projected electronic density of states of: (a) rutile-MgH_2, (b) trirutile-Mg_3H_6, (c) $FeMg_2H_6$, (d) $CoMg_2H_6$, (e) $NiMg_2H_6$, (f) $PdMg_2H_6$, (g) $PtMg_2H_6$.